
Proof of Therapeutic Efficacy of a ^{177}Lu -Labeled Neurotensin Receptor 1 Antagonist in a Colon Carcinoma Xenograft Model

Jörg Schulz*¹, Martin Rohracker*¹, Marvin Stiebler¹, Jürgen Goldschmidt², Franziska Stöber^{1,2}, Mercedes Noriega³, Anette Pethe¹, Mathias Lukas^{4,5}, Frank Osterkamp⁶, Ulrich Reineke⁶, Aileen Höhne⁶, Christiane Smerling⁶, and Holger Amthauer^{1,4}

¹Klinik für Radiologie und Nuklearmedizin, Otto-von-Guericke Universität, Magdeburg, Germany; ²Leibniz-Institut für Neurobiologie, Magdeburg, Germany; ³Institut für Pathologie, Universitätsklinik Hamburg-Eppendorf, Hamburg, Germany; ⁴Department of Nuclear Medicine, Charité-Universitätsmedizin Berlin, Berlin, Germany; ⁵Siemens Healthcare GmbH, Erlangen, Germany; and ⁶3B Pharmaceuticals GmbH, Berlin, Germany

See an invited perspective on this article on page 934.

Increased expression of neurotensin receptor 1 (NTR1) has been shown in a large number of tumor entities such as pancreatic or colon carcinoma. Hence, this receptor is a promising target for diagnostic imaging and radioligand therapy. Using the favorable biodistribution data of the NTR1-targeting agent ^{111}In -3BP-227, we investigated the therapeutic effect of its ^{177}Lu -labeled analog on the tumor growth of NTR1-positive HT29 colon carcinoma xenografts. **Methods:** 3BP-227 was labeled with ^{177}Lu . To assess its biodistribution properties, SPECT and CT scans of HT29-xenografted nude mice injected with ^{177}Lu -3BP-227 were acquired, and ex vivo tissue activity was determined. To evaluate therapeutic efficacy, 2 groups of mice received the radiopharmaceutical in a median dose of either 165 MBq (129–232 MBq, $n = 10$) or 110 MBq (82–116 MBq, $n = 10$), whereas control mice were injected with vehicle ($n = 10$). Tumor sizes and body weights were monitored for up to 49 d. Renal function and histologic morphology were evaluated. **Results:** Whole-body SPECT/CT images allowed clear tumor visualization with low background activity and high tumor-to-kidney and -liver ratios. Ex vivo biodistribution data confirmed high and persistent uptake of ^{177}Lu -3BP-227 in HT29 tumors (19.0 ± 3.6 vs. 2.7 ± 1.6 percentage injected dose per gram at 3 and 69 h after injection, respectively). The application of ^{177}Lu -3BP-227 resulted in a distinct delay of tumor growth. Median tumor doubling time for controls was 5.5 d (interquartile range [IQR], 2.8–7.0), compared with 17.5 d (IQR, 5.5–22.5 d) for the 110-MBq and 41.0 d (IQR, 27.5–55.0) for the 165-MBq group. Compared with controls, median relative tumor volume at day 23 after injection was reduced by 55% ($P = 0.034$) in the 110-MBq and by 88% ($P < 0.01$) in the 165-MBq group. Renal histology and clinical chemistry results did not differ between radiotherapy groups and controls, suggesting absence of therapy-induced acute renal damage. **Conclusion:** These data demonstrate that the novel NTR1-targeting theranostic agent 3BP-227 is an effective and promising candidate for radioligand therapy, with a favorable preliminary safety profile and high potential for clinical translation.

Key Words: NTR1 radiotracer; xenograft; SPECT/CT; theranostic; oncology

J Nucl Med 2017; 58:936–941

DOI: 10.2967/jnumed.116.185140

The successful diagnosis and therapy of somatostatin receptor-positive gastroenteropancreatic neuroendocrine tumors with ^{177}Lu - and ^{90}Y -labeled somatostatin analogs (1,2) demonstrate the high potential of neuropeptide receptor-based imaging and radioligand therapy (RLT). Because the range of somatostatin receptor-positive tumor entities is limited, other neuropeptide receptor systems such as the neurotensinergic system have been evaluated as targets for RLT. Neurotensin receptors (NTRs) mediate the effects of the neuropeptide hormone neurotensin, which acts as neuromodulator and peripherally as para- and endocrine factor in the gastrointestinal system (3). Physiologically, NTRs are mainly expressed in the central nervous as well as intestinal and hepatic system (4). Of the 3 known NTR subtypes, NTR1 is the primary mediator of neurotensin signaling because of its subnanomolar affinity to its natural ligand.

In colon carcinoma, breast cancer, and pancreatic adenocarcinoma, NTR1 expression has been associated with neoplastic progression (5–8). Furthermore, autoradiographic studies have shown that NTR1 is expressed in pancreatic adenocarcinoma in high densities of 10^3 – 10^4 dpm/mg in primary tumors (9) and metastases (8). Ewing's sarcoma, small cell lung cancer, and medullary thyroid carcinoma express similar densities, although a few individual tumors express receptor densities below 10^3 dpm/mg (10). These receptor densities are in a range similar to the somatostatin receptor subtype 2 (sst2) densities found in neuroendocrine tumors when tested autoradiographically using an sst2 agonist (11). Therefore, NTR1-targeting RLT for NTR1-expressing tumors may become a therapy similar in effectiveness to today's use of somatostatin analog-based RLT for neuroendocrine tumors.

An approximately 10-fold-higher number of binding sites has been demonstrated in various tumor entities using an sst2 antagonist than using an sst2 agonist (12). Several other studies have also revealed higher numbers of binding sites and increased tumor uptake for radiolabeled somatostatin and gastrin-releasing peptide receptor antagonists compared with agonists (13–15), which can be explained by the recognition of more conformational receptor states

Received Oct. 4, 2016; revision accepted Feb. 5, 2017.

For correspondence or reprints contact: Holger Amthauer, AB Klinische Nuklearmedizin, Klinik für Nuklearmedizin, Campus Virchow-Klinikum, Charité-Universitätsmedizin Berlin, Augustenburger Platz 1, 13353 Berlin, Germany.

E-mail: holger.amthauer@charite.de

*Contributed equally to this work.

Published online Mar. 2, 2017.

COPYRIGHT © 2017 by the Society of Nuclear Medicine and Molecular Imaging.

by the antagonist than the agonist (16). Hypothesizing that antagonist-based NTR1-targeting radiotracers might exhibit better tumor-to-normal-tissue uptake ratios than previously reported agonistic agents (17,18), Osterkamp et al. decided to modify the known NTR1 antagonist SR142948A (19,20) to allow attachment of the chelator DOTA (21). This strategy allows the formation of highly stable complexes with metal radionuclides such as ^{111}In , ^{68}Ga , ^{90}Y , and ^{177}Lu , and therefore enables use of the novel antagonistic derivatives as theranostic agents for a wide range of clinical applications such as SPECT or PET and RLT. We reported recently the favorable biodistribution profiles of the ^{111}In -labeled NTR1 antagonists 3BP-227 and 3BP-228, exhibiting high tumor and low normal-tissue uptake, with 3BP-227 yielding a more persistent tumor uptake (22). The aim of this follow-up study was to evaluate the antitumoral effect of ^{177}Lu -labeled 3BP-227 in the standard xenograft model in NTR1-targeted RLT, subcutaneous HT29 colon carcinoma tumors, and ultimately to gauge its potential for clinical translation.

MATERIALS AND METHODS

Radiolabeling

3BP-227 (35–40 μg) in buffer (0.4 M acetate, 0.325 M gentisic acid, pH 5) was incubated with 2.0–3.1 GBq of $^{177}\text{LuCl}_3$ (in 0.04 M HCl; Isotope Technologies Garching GmbH). The mixture was heated at 95°C for 30 min. After being cooled, the product was analyzed by thin-layer and high-performance liquid chromatography as previously described (22) and formulated in 0.9% NaCl for intravenous administration.

Cell Culture and Tumor Model

NTR1-positive HT29 human colorectal carcinoma cells (European Collection of Authenticated Cell Cultures and Cell Lines Services) (23) were grown in McCoy's 5A modified medium (Biochrom) supplemented with 10% fetal calf serum, 2 mM L-glutamine, penicillin (10,000 U/mL), and streptomycin (10 mg/mL) at 37°C in 5% CO_2 .

Experiments were approved by the local animal welfare committee and performed according to national regulations. Mice were kept in an individually ventilated cage system under standard conditions with food and water ad libitum. HT29 cells ($2\text{--}3 \times 10^6$ cells) were inoculated subcutaneously in the flank of 6- to 8-wk-old athymic $\nu\text{-}\nu$ female mice (Nude-Foxn1tm; Harlan Laboratories).

SPECT/CT Imaging

SPECT/CT whole-body imaging was performed at 3, 20, 45, 69, and 93 h after injection of ^{177}Lu -3BP-227 in 2 mice (159.7 and 130.7 MBq, respectively). Images were acquired under isoflurane anesthesia (1%–2% isoflurane in 2:1 $\text{O}_2\text{:N}_2\text{O}$ volume ratio) with a 4-head NanoSPECT/CT scanner (Mediso Ltd.). CT and SPECT were coregistered. Whole-body CT scans were acquired at pixel sizes of 192 μm and reconstructed with the manufacturer's software (InVivoScope 1.43) at isotropic voxel sizes of 200 μm . Whole-body SPECT scans were acquired using a multipinhole collimator set (SCIVIS), each collimator with 9 pinholes (1.4-mm pinhole diameter, ≤ 1.0 mm nominal resolution). Photopeaks were set to the default values of the NanoSPECT for ^{177}Lu (57, 113, and 208 keV, each $\pm 10\%$). Acquisition time was 60 min. SPECT scans were reconstructed using the manufacturer's software (HiSPECT; SCIVIS) at isotropic voxel output sizes of 300–600 μm , depending on counting rates.

Ex Vivo Biodistribution Study

Mice were injected with 4.0 ± 0.7 MBq of ^{177}Lu -3BP-227 and sacrificed under isoflurane anesthesia 3, 20, or 69 h later ($n = 5$ per time point). Tissues of interest and urine were removed and weighed, and their activity content was determined by well-counter measurement. Tissue counts and injected dose for individual mice were decay-corrected

to the time of euthanasia. Tissue uptake is expressed as the percentage injected dose per gram of tissue (%ID/g).

RLT

Radiopharmaceutical or vehicle injection was performed 7 d after tumor cell inoculation (day 0). At this time, tumors had reached a mean volume of 90 mm^3 . Mice were divided into 3 groups of 10, receiving either a median dose of 110 MBq (82–116 MBq) or 165 MBq (129–232 MBq) of ^{177}Lu -3BP-227 or vehicle (0.9% NaCl) via a lateral tail vein. One mouse in the 165-MBq group had to be excluded from analysis because of a failed injection. Tumor measurements by digital caliper, determinations of body weight, and assessments of clinical status were performed 3 times a week beginning at the day of active agent or vehicle injection (day 0). Tumor volume was calculated according to the formula $V = (\pi/6)LW^2$ (L = largest, W = shortest diameter of the tumor). Because the average tumor sizes in the 3 groups were not equal on day 0, individual tumor measurements were normalized to their initial value at day 0 and are presented as relative tumor volume ($V_{\text{day after injection}}/V_0$). Endpoint criteria were defined as relative body weight (body weight at day after injection divided by weight on day 0) < 0.85 ; tumor volume $> 1,500$ mm^3 or largest diameter ≥ 15 mm; exulceration or invasive growth of the tumor; and clinical abnormalities such as apathy, labored respiration, impaired movement, or abnormal posture. The study was terminated after a maximum observation time of 49 d.

Kidney Function and Morphology

To investigate potential induction of renal damage by ^{177}Lu -3BP-227, kidney sections were histologically examined. For this purpose, the kidneys of 3 mice of the 165-MBq, 110-MBq, and control groups were collected after they reached endpoint criteria or the end of the investigation period. Organs were fixed in 4% paraformaldehyde and embedded in paraffin. Dewaxed sections were either stained with periodic acid–Schiff reagent, hematoxylin and eosin, or Masson Trichrom staining. Specimens were evaluated by a trained nephropathologist. Furthermore, blood samples were taken via heart puncture directly after euthanasia. Serum concentrations of creatinine and urea were measured using standard techniques of clinical chemistry. Neutrophil gelatinase-associated lipocalin and cystatin C concentrations were determined by enzyme-linked immunosorbent assay (Mouse NGAL ELISA Kit [BioPorto Diagnostics A/S]; Mouse Cystatin C ELISA Kit [Boster Biotechnology Co., Inc.]) following the manufacturer's instructions.

Data Analysis

OsiriX MD (open source version 1.3, 64-bit) was used to analyze SPECT/CT data. Regions of interest for kidneys and tumors were drawn manually on transaxial CT slices. Volumes of interest were compiled of 2-dimensional regions of interest delineating the entire extent of each examined tissue and transferred to corresponding SPECT slices for quantification of counts in the volumes of interest.

Dosimetric calculations for selected tissues were performed using the sphere model of OLINDA/EXM software (version 1.1) (24) and monoexponential fitting of kinetic data. The tumor mass was assumed to be constant using the barycenter of the mass over time function. The resulting absorbed doses have to be considered rough estimates because of the limited number of time points and the imperfect tumor's spheric shape.

SPSS Statistics (83-bit version 22.0.0.0; IBM) was used for statistical analysis and data visualization. Statistical analysis of differences of medians of relative tumor volume, tumor doubling times, relative body weight, and kidney parameters was performed using the Kruskal–Wallis test followed by the Mann–Whitney U test for multiple comparisons or Mann–Whitney U test for analyzing differences between 2 groups. For evaluation of the results of the RLT study, a Kaplan–Meier analysis and log-rank tests were performed. The endpoint was defined as reaching a

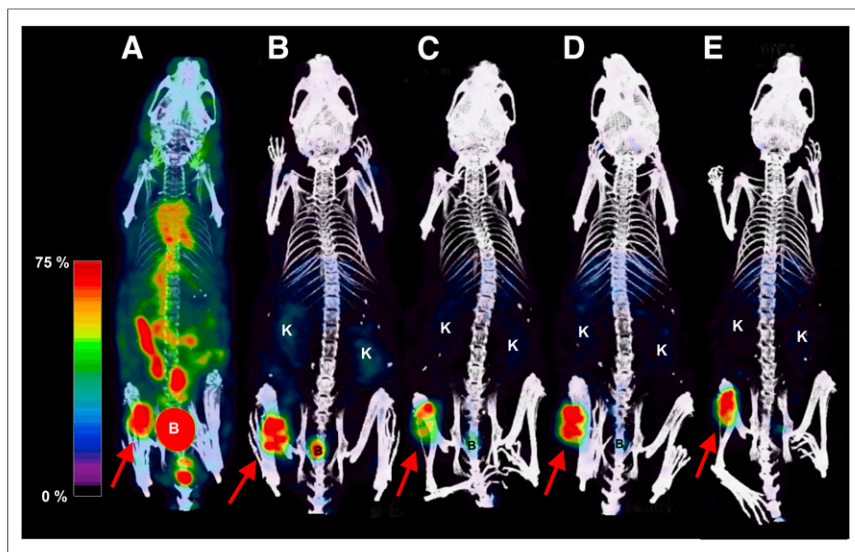


FIGURE 1. Coregistered whole-body SPECT/CT scans of a single female nude mouse grafted with HT29 tumor cells acquired 3 (A), 20 (B), 45 (C), 69 (D), and 93 (E) h after injection of 130.7 MBq of ^{177}Lu -3BP-227. Arrows show HT29 tumors. SPECT data were scaled to 0%–75% of maximum count value in the tumor of the respective dataset. B = Urinary bladder; K = Kidney.

relative tumor volume of 2 or greater. Differences of P values less than 0.05 were considered statistically significant.

RESULTS

Radiolabeling

^{177}Lu radiolabeling yields of 3BP-227 were 95% or more based on thin-layer and high-performance liquid chromatography. Specific activities were 56.5 for the imaging and 59.9 MBq/nmol for the biodistribution study, and 59.3 MBq/nmol for the 110-MBq group and 87.6 MBq/nmol for the 165-MBq group in the therapy setting.

SPECT/CT Imaging

^{177}Lu -3BP-227-SPECT/CT imaging of HT29-xenografted nude mice visualized the tumor clearly. At 3 h after injection, distinct background activity was still present, representing circulating radiotracer as well as urogenital and intestinal accretion (Fig. 1). By 20, 45, 69, and 93 h after injection tumor uptake clearly exceeded uptake in the kidneys and liver. The tumor-to-kidney activity ratio of the animal depicted in Figure 1 continuously increased from 1.19 at 3 h after injection to 5.66 at 93 h after injection (3.26 at 20 h after injection, 3.89 at 45 h after injection, 4.65 at 69 h after injection). The tumor-to-liver activity ratio was 1.35 at 3 h after injection, rising to a constantly high level in the following acquisitions (3.20 at 20 h after injection, 3.21 at 45 h after injection, 3.31 at 69 h after injection, 3.76 at 93 h after injection). These data indicate a slower washout from tumor than from renal and hepatic tissue. Tumor uptake was persistent—at 93 h after injection, still 34% of the decay-corrected activity determined at the first acquisition was still present in the tumor. The second mouse in the imaging study showed a similar distribution profile (Supplemental Fig. 1; supplemental materials are available at <http://jnm.snmjournals.org>).

Ex Vivo Biodistribution Study

The ex vivo biodistribution data for ^{177}Lu -3BP-227 confirmed a high and persistent tumor accumulation (Fig. 2; Supplemental Table 1). HT29 uptake at 3 h after injection was 19.0 ± 3.6

%ID/g, 8.6 ± 4.0 %ID/g at 20 h after injection, and 2.7 ± 1.6 %ID/g at 69 h after injection. A mean absorbed radiation dose of 830 mGy/MBq of ^{177}Lu was estimated for the tumor. Low and over time decreasing activity was measured in the kidneys. Tumor-to-kidney ratios rose from 5.2 ± 2.5 at 3 h after injection to 6.3 ± 4.3 at 20 h and 15.9 ± 19.3 at 69 h after injection, respectively, indicating a faster washout of these critical organs than from target tissue. At each time point after injection, tumor uptake exceeded uptake in all other examined tissues considerably. In our dosimetry estimation this translated into low extrapolated human body and organ doses (Supplemental Table 2).

RLT

Two groups of HT29-grafted nude mice were injected with a median dose of either 110 MBq (82–116 MBq) or 165 MBq (129–232 MBq) of ^{177}Lu -3BP-227, corresponding to an average injected mass of approximately 1.9 nmol in both groups. Tu-

mor volumes of control animals having received 0.9% NaCl vehicle injections instead of ^{177}Lu -3BP-227 increased rapidly, with a median doubling time of 5.5 d (interquartile range, 2.8–7.0 d) (Fig. 3). Treatment with ^{177}Lu -3BP-227 induced a marked slowing of tumor growth. In the 110-MBq group, the median doubling time was 17.5 d (interquartile range, 5.5–22.5 d) ($P = 0.022$ vs. control) and in the 165-MBq group it was prolonged to 41.0 d (interquartile range, 27.5–55.0 d) ($P < 0.001$ vs. control; $P = 0.015$ vs. 110-MBq group). At day 23 after injection, most animals in the control group reached tumor volumes that necessitated euthanasia. At this time, median relative tumor volume in the 110-MBq group was reduced by 55% ($P = 0.034$) and by 88% in the 165-MBq group ($P < 0.01$) compared with controls. Differences in relative tumor volume between the 110-MBq group and controls were statistically significant from day 7 after injection ($P < 0.05$). Between the 165-MBq group and controls, differences were statistically significant from day 4 after injection ($P < 0.01$). Application of 110 MBq of ^{111}Lu -3BP-227 stabilized tumor size up to a median relative tumor volume level of approximately 2 until day 20 after injection, whereupon tumor growth proceeded similar to controls. The observation of animals receiving 110 MBq was terminated at day 38 after injection when most of the mice reached endpoint criteria. In comparison to the 110-MBq group, median relative tumor volume in the 165-MBq group was 89% lower at this time ($P = 0.009$). The effect of 165 MBq of ^{177}Lu -3BP-227 was more persistent, with a median relative tumor volume of only 2.4 by day 49 after injection. Absolute tumor volume data are shown in Supplemental Figure 2.

Kaplan–Meier analysis (Fig. 3) was performed to demonstrate the tumor growth behavior of individual mice. Four of 9 mice in the 165-MBq group and 1 animal of 10 in the 110-MBq group did not reach the endpoint, set at reaching twice the initial tumor volume. Log-rank tests showed a significantly increased tumor doubling time after application of ^{177}Lu -3BP-227 in comparison with controls (110 MBq vs. control $P = 0.006$, 165 MBq vs. control $P < 0.001$). Application of 165 MBq of the compound had a significantly stronger effect than 110 MBq ($P = 0.013$).

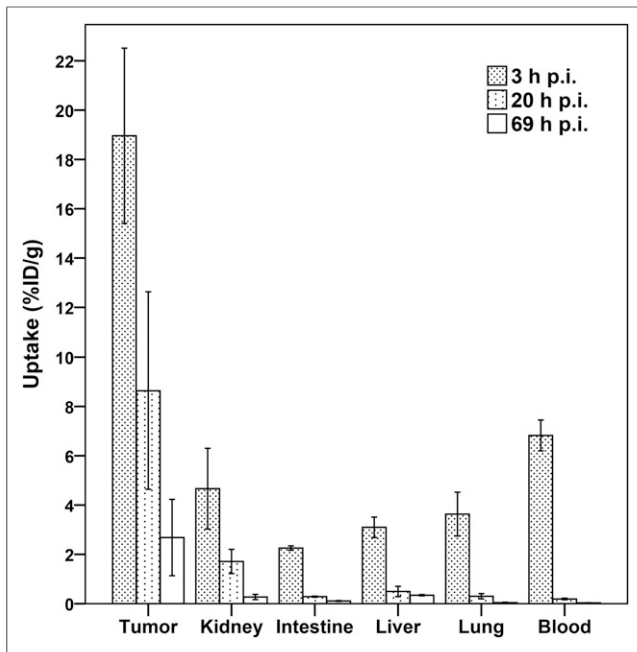


FIGURE 2. Uptake of ¹⁷⁷Lu-3BP-227 in selected tissues 3, 20, and 69 h after injection (mean %ID/g ± SD). *n* = 5 mice per time point. p.i. = after injection.

Evaluation of Acute Toxicity

When the relative body weight of the 3 groups was compared, 165- and 110-MBq groups showed an intermittent weight loss of 7.2% ($P = 0.001$) and 4.7% ($P < 0.001$), respectively, in relation to the controls at day 3–5 after injection. At day 7 after injection, the intervention groups recovered their initial body weight. Hereafter, progression of body mass of the 165-MBq group and the control converged, with no statistically significant differences, whereas body weights of the 110-MBq group initially stayed stable but then increased continuously, remaining, however, on an overall lower level than the other 2 groups (Supplemental Fig. 3).

None of the examined functional kidney parameters revealed a significant or relevant change for both 165- and 110-MBq groups

versus controls (Fig. 4). No pathologic abnormalities, such as tubular damage, thrombotic microangiopathy, interstitial nephritis, or glomerulonephritis, were detectable. No histologic differences between the kidneys of ¹⁷⁷Lu-3BP-227- and vehicle-injected mice were visible.

DISCUSSION

This study presents the first, to our knowledge, evaluation of the therapeutic effect of an NTR1-antagonistic radiopharmaceutical. 3BP-227 is equipped with a DOTA chelator, allowing incorporation of a range of diagnostic and therapeutic metal radionuclides (e.g., ⁶⁸Ga for PET, ¹¹¹In for SPECT, ⁹⁰Y and ¹⁷⁷Lu for RLT). This enables use of 3BP-227 as a theranostic agent, that is, 3BP-227 labeled with a diagnostic radionuclide could be used to assess NTR1 expression and suitability for 3BP-227-based RLT in an individualized precision medicine approach. This is important because NTR1 expression in different tumor types can vary substantially (8,9,10,25), and patient selection is warranted for a successful treatment.

On the basis of its advantageous physical properties for RLT especially of smaller tumors (half-life, 6.7 d; maximum energy, 0.5 MeV, corresponding to tissue penetration depth of 2 mm), we chose the β -emitter ¹⁷⁷Lu as the therapeutic radionuclide for this study. Consistent with our previous report on the theranostic potential of 3BP-227 (22), the biodistribution profile of ¹⁷⁷Lu-labeled 3BP-227 in NTR1-positive HT29 tumor-bearing mice confirmed high tumor accumulation and low uptake in normal tissues, leading to favorable tumor-to-kidney activity ratios (e.g., 3.2 at 20 h after injection). Persistent uptake of radiopharmaceuticals in normal tissues can compromise their therapeutic applicability because of potential radiotoxicity. In particular, the accumulation of peptide radiopharmaceuticals in the kidneys has been described and may cause dose-limiting renal toxicity (26). The observed high tumor-to-kidney uptake ratios for ¹⁷⁷Lu-3BP-227 suggest that therapeutically effective doses of the radiopharmaceutical are unlikely to cause intolerable radiation damage to the kidneys.

Interestingly, tumor uptake of ¹⁷⁷Lu-3BP-227 appeared to be significantly higher than of its ¹¹¹In-labeled analog (22) (e.g., $P = 0.02$ at 20 and 24 h after injection, respectively). This observation cannot be attributed to differences in affinity: the half maximal inhibitory concentration of both compounds has been determined to be similar in an in vitro functional calcium assay (5.35 nM for ^{nat}In- vs. 5.95 nM for ^{nat}Lu-3BP-227) as well as in a radioligand binding assay (0.76 nM for ^{nat}In- vs. 0.59 nM for ^{nat}Lu-3BP-227) (21). More likely the discrepancy in ¹⁷⁷Lu- versus ¹¹¹In-3BP-227 uptake in tumors as well as other tissues is due to variation in experimental parameters such as batch-to-batch variability of xenografts and administered mass dose, and a head-to-head comparison would be necessary to determine whether there are any true differences in the biodistribution of 3BP-227 labeled with different radiometals.

Administration of a single therapeutic dose of ¹⁷⁷Lu-3BP-227 to HT29-xenografted mice led to statistically significant and persistent tumor growth inhibition with a distinct dose-dependent response. A more than 3-fold increase of tumor doubling time corresponding

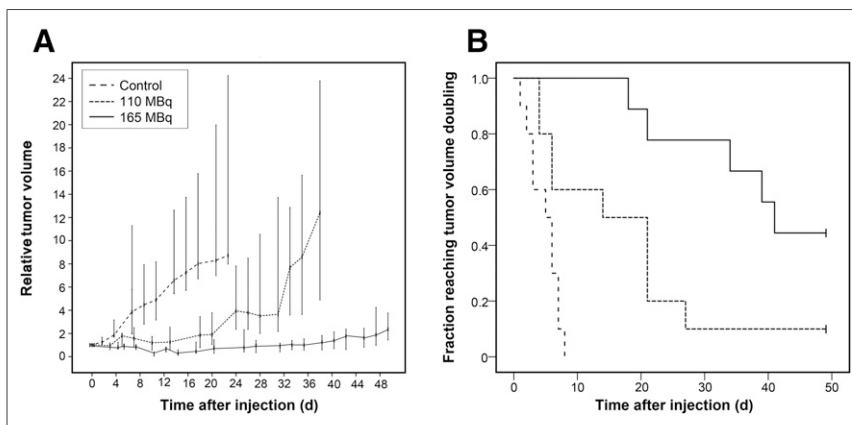


FIGURE 3. (A) Therapeutic effect of ¹⁷⁷Lu-3BP-227 in female nude mice grafted with HT29 cells. Tumor volume data are normalized to measurement at day of ¹⁷⁷Lu-3BP-227 injection and represented as median and interquartile range. (B) Kaplan–Meier plot showing tumor progression of HT29 in same study. Endpoint was set at reaching relative tumor volume of ≥ 2 . Control: *n* = 10; 165-MBq group: *n* = 9; 110-MBq group: *n* = 10.

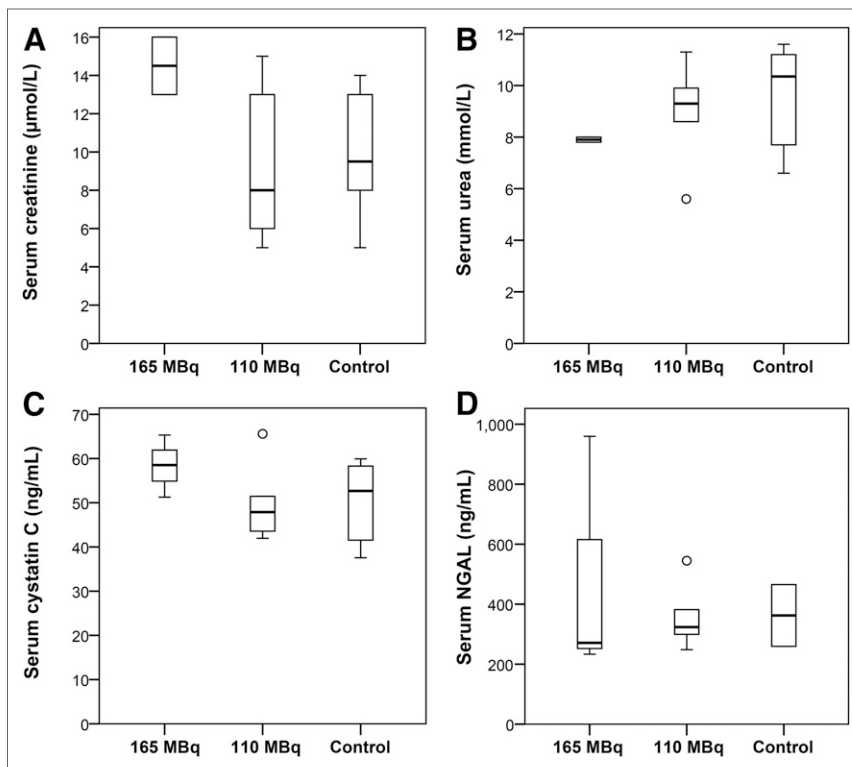


FIGURE 4. Serum concentrations of functional kidney biomarkers—creatinine (A), urea (B), cystatin C (C), and neutrophil gelatinase–associated lipocalin (NGAL) (D)—of female nude mice grafted with HT29 cells obtained after injection of median dose of 165 or 110 MBq of ^{177}Lu -3BP-227 or 0.9% NaCl as control. Sample sizes (165-MBq group/110-MBq group/control)—2/5/6 (A), 2/5/6 (B), 3/5/6 (C), and 3/5/2 (D). Statistical analysis comparing biomarker concentrations was performed by Kruskal–Wallis test, with no significant differences detected.

to a tumor growth delay of approximately 2 wk was observed for the 110-MBq group compared with controls. The antitumor effect was even more pronounced in the 165-MBq group, with a more than 7-fold increase in tumor doubling time and a tumor growth delay of more than 5 wk. So far, such a high degree of tumor growth inhibition has not been achieved with NTR1-targeted radiotherapeutics. Comparable studies investigating the antitumoral potential of NTR1-agonistic radioligands were performed using peptidic neurotensin analogs based on the biologically active sequence 8-13. García-Garayoa et al. examined the metabolically stabilized neurotensin derivative (NHis)Ac-Arg-(N-CH₃)-Arg-Pro-Dmt-Tle-Leu (NT-XIX), the $^{99\text{m}}\text{Tc}$ -labeled version of which displayed a promising biodistribution pattern for theranostic applications, with tumor-to-kidney ratios of 1.9–2.7 between 1.5 and 24 h after injection (17). Labeled with ^{188}Re , a significant inhibition of HT29 tumor growth by this peptide was shown in the first week after administration of the first fraction. In subsequent weeks, however, tumor growth did not differ significantly between therapy and control groups, resulting in only marginally increased tumor doubling times under ^{188}Re -NT-XIX treatment. Maschauer et al. investigated the therapeutic efficacy of the ^{177}Lu -labeled, metabolically stabilized neurotensin derivative Nlys-Lys-Pro-Tyr-Tle-Leu (^{177}Lu -NT127) (18). Compared with controls, a significant reduction of HT29 tumor volume of 50% was shown 4 wk after the application of a single dose of 50 MBq. However, relatively high tracer uptake in excretory organs was observed, leading to tumor-to-kidney ratios as low as 0.03–0.04 between 1 and 24 h after injection. This unspecific accumulation led

to significant radiation-induced damage to liver and kidney tissues, hindering clinical translation of ^{177}Lu -NT127-RLT.

In contrast to previously reported neurotensin derivatives, the medium-sized NTR1 antagonist ^{177}Lu -3BP-227 elicits a promising therapeutic effect with a favorable biodistribution profile. In line with the observed biodistribution pattern showing low accumulation and absorbed radiation doses in excretory organs, there was no evidence of radiation-induced acute side effects to the kidneys after administration of ^{177}Lu -3BP-227. Our dosimetry estimates show that even when administering a rather high cumulative patient dose of 50 GBq of ^{177}Lu -3BP-227, the absorbed radiation dose for the kidneys should be only around 6 Gy, which is far below the postulated 23 Gy threshold for increased probability of developing severe late kidney damage. Although we have observed cross-reactivity of 3BP-227 with murine and human NTR1 (Christiane Smerling and Frank Osterkamp, unpublished data), under- or overestimation of renal damage in patients through extrapolation from the xenograft model is still possible because of potential species differences in NTR1 kidney expression or radiotracer pharmacokinetics. The observed reduction in body weight gain was only transient and not directly dose-dependent. Taken together, these results suggest that ^{177}Lu -3BP-227, while having a statistically significant inhibitory

effect on tumor growth, induces no overt signs of acute nephrotoxicity at the doses studied. However, radiation nephropathy has been observed to occur late (>6 mo) after RLT (27,28). Long-term toxicity as well as comprehensive dosimetry studies are needed to evaluate whether measures for kidney protection such as dose fractionation or coadministration of renoprotective agents are necessary in conjunction with ^{177}Lu -3BP-227 therapy. Furthermore, considering the relatively high initial blood-pool activity of ^{177}Lu -3BP-227, its hematotoxic safety profile needs to be assessed in future studies.

CONCLUSION

This study demonstrates the therapeutic potential of ^{177}Lu -labeled 3BP-227. ^{177}Lu -3BP-227 inhibited HT29 tumor growth to a high degree and in a dose-dependent manner without significant acute toxic effects on normal tissues. The favorable properties for both patient stratification and RLT applications underline the high potential of 3BP-227 as a theranostic agent for clinical translation. Further preclinical evaluations, for example, evaluation in other tumor models as well as multidose, detailed dosimetry and toxicity studies, are currently ongoing and paving the way toward clinical studies of the therapeutic efficacy of ^{177}Lu -3BP-227 in cancer patients.

DISCLOSURE

This work was supported by the KMU Innovativ program of the German Federal Ministry of Education and Research (BMBF,

principal investigator Christiane Smerling, grant no. 0315865) and the Foundation of German Business (SDW; Jörg Schulz). No other potential conflict of interest relevant to this article was reported.

ACKNOWLEDGMENT

We thank Ines Bodewald for her expert technical assistance.

REFERENCES

1. Reubi JC, Schär JC, Waser B, et al. Affinity profiles for human somatostatin receptor subtypes SST1-SST5 of somatostatin radiotracers selected for scintigraphic and radiotherapeutic use. *Eur J Nucl Med*. 2000;27:273–282.
2. Alonso-Gordo T, Capdevila J, Grande E. GEP-NETs update: biotherapy for neuroendocrine tumours. *Eur J Endocrinol*. 2015;172:R31–R46.
3. Vincent JP, Mazella J, Kitabgi P. Neurotensin and neurotensin receptors. *Trends Pharmacol Sci*. 1999;20:302–309.
4. Johnson LR. *Physiology of the Gastrointestinal Tract, Two Volume Set*. Burlington, MA: Elsevier Science; 2012.
5. Dupouy S, Viardot-Foucault V, Alifano M, et al. The neurotensin receptor-1 pathway contributes to human ductal breast cancer progression. *PLoS One*. 2009;4:e4223.
6. Gui X, Liu S, Meng Z, Gao Z. Neurotensin receptor 1 (NTSR1) overexpression in breast carcinomas is common and independent of ER/PR/Her2 expression. *J Cancer Ther*. 2013;4(7A):12–17.
7. Gui X, Guzman G, Dobner PR, Kadkol SS. Increased neurotensin receptor-1 expression during progression of colonic adenocarcinoma. *Peptides*. 2008;29:1609–1615.
8. Körner M, Waser B, Strobel O, Büchler M, Reubi JC. Neurotensin receptors in pancreatic ductal carcinomas. *EJNMMI Res*. 2015;5:17.
9. Reubi JC, Waser B, Friess H, Büchler M, Laissue J. Neurotensin receptors: a new marker for human ductal pancreatic adenocarcinoma. *Gut*. 1998;42:546–550.
10. Reubi JC, Waser B, Schaer JC, Laissue JA. Neurotensin receptors in human neoplasms: high incidence in Ewing's sarcomas. *Int J Cancer*. 1999;82:213–218.
11. Reubi JC, Waser B. Concomitant expression of several peptide receptors in neuroendocrine tumours: molecular basis for in vivo multireceptor tumour targeting. *Eur J Nucl Med Mol Imaging*. 2003;30:781–793.
12. Reubi JC, Waser B, Maecke HR, Rivier JE. Highly increased ¹²⁵I-JR11 antagonist binding in vitro reveals novel indications for sst2 targeting in human cancers. *J Nucl Med*. 2017;58:300–306.
13. Dash A, Chakraborty S, Pillai MR, Knapp FF Jr. Peptide receptor radionuclide therapy: an overview. *Cancer Biother Radiopharm*. 2015;30:47–71.
14. Wild D, Fani M, Behe M, et al. First clinical evidence that imaging with somatostatin receptor antagonists is feasible. *J Nucl Med*. 2011;52:1412–1417.
15. Cescaio R, Maina T, Nock B, et al. Bombesin receptor antagonists may be preferable to agonists for tumor targeting. *J Nucl Med*. 2008;49:318–326.
16. Sleight AJ, Stam NJ, Mutel V, Vanderheyden PM. Radiolabelling of the human 5-HT_{2A} receptor with an agonist, a partial agonist and an antagonist: effects on apparent agonist affinities. *Biochem Pharmacol*. 1996;51:71–76.
17. García-Garayo E, Blauenstein P, Blanc A, Maes V, Tourwé D, Schubiger PA. A stable neurotensin-based radiopharmaceutical for targeted imaging and therapy of neurotensin receptor-positive tumours. *Eur J Nucl Med Mol Imaging*. 2009;36:37–47.
18. Maschauer S, Ruckdeschel T, Tripal P, et al. In vivo monitoring of the antiangiogenic effect of neurotensin receptor-mediated radiotherapy by small-animal positron emission tomography: a pilot study. *Pharmaceuticals (Basel)*. 2014;7:464–481.
19. Gully D, Canton M, Boiegrain R, et al. Biochemical and pharmacological profile of a potent and selective nonpeptide antagonist of the neurotensin receptor. *Proc Natl Acad Sci USA*. 1993;90:65–69.
20. Gully D, Labeuw B, Boiegrain R, et al. Biochemical and pharmacological activities of SR 142948A, a new potent neurotensin receptor antagonist. *J Pharmacol Exp Ther*. 1997;280:802–812.
21. Osterkamp F, Smerling C, Reineke U, Haase C, Ungewiss J, inventors; 3BP Pharmaceuticals GmbH, assignee. Neurotensin receptor ligands. European patent application EP20120008208. December 7, 2012.
22. Schulz J, Rohracker M, Stiebler M, et al. Comparative evaluation of the biodistribution profiles of a series of nonpeptidic neurotensin receptor-1 antagonists reveals a promising candidate for theranostic applications. *J Nucl Med*. 2016;57:1120–1123.
23. Vita N, Laurent P, Lefort S, et al. Cloning and expression of a complementary DNA encoding a high affinity human neurotensin receptor. *FEBS Lett*. 1993;317:139–142.
24. Stabin MG, Sparks RB, Crowe E. OLINDA/EXM: the second-generation personal computer software for internal dose assessment in nuclear medicine. *J Nucl Med*. 2005;46:1023–1027.
25. Souazé F, Dupouy S, Viardot-Foucault V, et al. Expression of neurotensin and NT1 receptor in human breast cancer: a potential role in tumor progression. *Cancer Res*. 2006;66:6243–6249.
26. Lambert B, Cybulla M, Weiner SM, et al. Renal toxicity after radionuclide therapy. *Radiat Res*. 2004;161:607–611.
27. Valkema R, Pauwels SA, Kvolts LK, et al. Long-term follow-up of renal function after peptide receptor radiation therapy with ⁹⁰Y-DOTA(0),Tyr(3)-octreotide and ¹⁷⁷Lu-DOTA(0), Tyr(3)-octreotate. *J Nucl Med*. 2005;46(suppl 1):83S–91S.
28. Rolleman EJ, Krenning EP, Bernard BF, et al. Long-term toxicity of [¹⁷⁷Lu-DOTA(0),Tyr(3)]octreotate in rats. *Eur J Nucl Med Mol Imaging*. 2007;34:219–227.